

Fermi surface and pseudogap in highly doped Sr_2IrO_4

Y. Alexanian,^{1,*} A. de la Torre,^{2,3} S. McKeown Walker,^{1,4} M. Straub,¹ G. Gatti,¹ A. Hunter,¹ S. Mandloi,¹ E. Cappelli,¹ S. Riccò,¹ F. Y. Bruno,⁵ M. Radovic,⁶ N. C. Plumb,⁶ M. Shi,⁶ J. Osiecki,⁷ C. Polley,⁷ T. K. Kim,⁸ P. Dudin,^{8,9} M. Hoesch,¹⁰ R. S. Perry,^{11,12} A. Tamai,¹ and F. Baumberger^{1,6}

¹*Department of Quantum Matter Physics, University of Geneva,
24 Quai Ernest-Ansermet, CH-1211, Geneva, Switzerland*

²*Department of Physics, Northeastern University, Boston, MA, 02115, USA*

³*Quantum Materials and Sensing Institute, Northeastern University, Burlington, MA, 01803 USA*

⁴*Laboratory of Advanced Technology, University of Geneva,
24 Quai Ernest-Ansermet, CH-1211, Geneva, Switzerland*

⁵*GFMC, Departamento de Física de Materiales, Universidad Complutense de Madrid, 28040 Madrid, Spain*

⁶*Swiss Light Source, Paul Scherrer Institut, CH-5232 Villigen PSI, Switzerland*

⁷*MAX IV Laboratory, Lund University, SE-211 00 Lund, Sweden*

⁸*Diamond Light Source, Harwell Campus, Didcot, OX11 0DE, United Kingdom*

⁹*Synchrotron SOLEIL, L'Orme des Merisiers, Saint Aubin-BP 48, 91192 Gif sur Yvette Cedex, France*

¹⁰*Deutsches Elektronen-Synchrotron DESY, Notkestraße 85, 22607 Hamburg, Germany*

¹¹*ISIS Pulsed Neutron and Muon Source, STFC Rutherford Appleton Laboratory,
Harwell Campus, Didcot, Oxon OX11 0QX, United Kingdom*

¹²*London Centre for Nanotechnology and Department of Physics and Astronomy,
University College London, London WC1E 6BT, United Kingdom*

(Dated: May 20, 2025)

The fate of the Fermi surface in bulk electron-doped Sr_2IrO_4 remains elusive, as does the origin and extension of its pseudogap phase. Here, we use high-resolution angle-resolved photoelectron spectroscopy (ARPES) to investigate the electronic structure of $\text{Sr}_{2-x}\text{La}_x\text{IrO}_4$ up to $x = 0.2$, a factor of two higher than in previous work. We find that the antinodal pseudogap persists up to the highest doping level, and thus beyond the sharp increase in Hall carrier density to $\simeq 1 + x$ recently observed above $x^* = 0.16$ [1]. This suggests that doped iridates host a unique phase of matter in which a large Hall density coexists with an anisotropic pseudogap, breaking up the Fermi surface into disconnected arcs. The temperature boundary of the pseudogap is $T^* \simeq 200$ K for $x = 0.2$, comparable to cuprates and to the energy scale of short range antiferromagnetic correlations in cuprates and iridates.

The pseudogap (PG) in hole doped cuprates is one of the most enigmatic properties of correlated electron systems. A pragmatic definition of a PG, adopted throughout this article, is the existence of a sharp suppression of spectral weight at low energy scales. ARPES experiments established that the cuprate PG is anisotropic and selectively suppresses the low-energy spectral weight near $(\pi, 0)$, leaving apparent Fermi arcs extending out from the node along the Brillouin zone diagonal [2, 3]. However, the origin of the PG and its relation with the rich phase diagram of cuprates remain controversial, not least because there is little thermodynamic evidence for a genuine phase transition at the critical doping p^* and temperature T^* where the PG closes [4–7]. When superconductivity is suppressed in high magnetic fields, several cuprate families show a strong peak in the electronic specific heat near p^* , in some cases accompanied by a $\log(1/T)$ dependence at low temperatures. Around the same doping level, the Hall carrier density increases from the doping p to $1 + p$ [8, 9]. Whether these signatures are caused by a quantum critical point associated with the closure of the PG remains debated.

The recent observation by Hsu *et al.* of similar anomalies in the electronic specific heat and Hall density in

the electron doped iridate $\text{Sr}_{2-x}\text{La}_x\text{IrO}_4$ provides complementary insight into these open questions [1]. Undoped Sr_2IrO_4 is a single band antiferromagnetic (AF) insulator, commonly described as a pseudospin $J_{\text{eff}} = 1/2$ Mott state [10–12], although other interpretations have been put forward [13]. A minimal model of electron doped Sr_2IrO_4 remarkably resembles that of hole doped cuprates [14]. ARPES experiments at low La (*i.e.* electron) doping revealed a PG with the same anisotropy in momentum space known from hole doped cuprates [15–17]. Crucially though, $\text{Sr}_{2-x}\text{La}_x\text{IrO}_4$ shows no signs of superconductivity up to the highest doping of $x = 0.2$ investigated so far [18]. On the other hand, short range AF spin correlations in $\text{Sr}_{2-x}\text{La}_x\text{IrO}_4$ closely reflect spin excitations in cuprates [19–22], although no charge or spin orders were found in iridates. These observations prompted suggestions that the PG in iridates is driven by magnetic fluctuations [1, 15].

Hsu *et al.* interpreted the anomalies in specific heat and Hall density as a signature of the closure of the PG at a critical La doping $x^* \simeq 0.16$ [1]. This is qualitatively consistent with an ARPES study of K surface doped Sr_2IrO_4 that found a transition from a pseudogapped regime to a conventional large Fermi surface (FS) around a K cover-

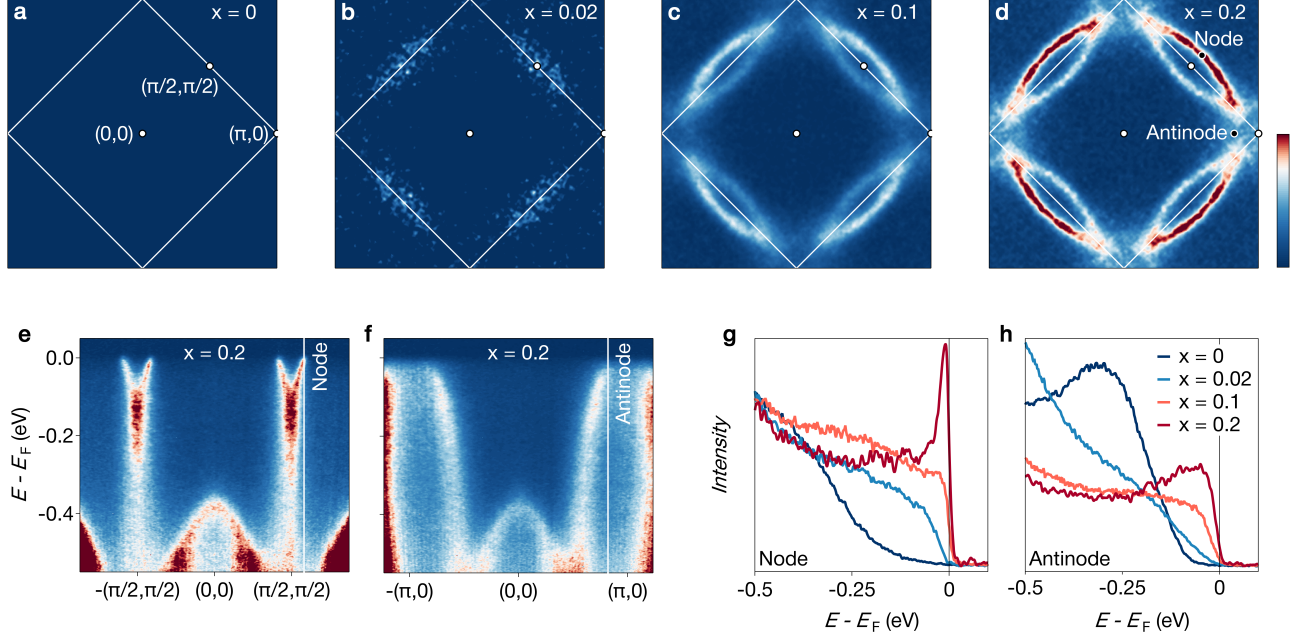


FIG. 1. **Collapse of the spin-orbit driven Mott insulating ground state and emergence of the pseudogap state in $\text{Sr}_{2-x}\text{La}_x\text{IrO}_4$.** **a-d** Fermi surfaces for $x = 0$, $x = 0.02$, $x = 0.1$, and $x = 0.2$, respectively. Data were measured at $T \approx 50$ K (**a,b**) and $T \approx 10$ K (**c,d**) with a photon energy $h\nu = 100$ eV and have been fourfold rotationally averaged. **e,f** ARPES band dispersion of $\text{Sr}_{1.8}\text{La}_{0.2}\text{IrO}_4$ along the nodal $(0,0) - (\pi, \pi)$ and antinodal $(0,0) - (\pi, 0)$ directions, illustrating the nodal-antinodal dichotomy. **g,h** Doping dependence of energy distribution curves (EDCs) at the nodal and antinodal positions indicated in **d-f**.

age of ~ 0.85 monolayer (ML) [23]. However, it is unclear whether the K/AF-insulator interface is representative of highly bulk doped samples, which are metallic and paramagnetic. In bulk electron doped samples there is thus far no direct evidence for a closure of the PG.

Here, we report high-resolution ARPES data from the same batch of $\text{Sr}_{2-x}\text{La}_x\text{IrO}_4$ samples studied by Hsu *et al.* [1]. We find that the electronic structure evolves smoothly across x^* . Quasiparticle coherence increases monotonously with doping while the nodal Fermi velocity is largely constant. Most importantly, the PG remains open up to at least $x = 0.2$ and thus beyond the Hall density crossover reported by Hsu *et al.* [1] at $x^* \approx 0.16$. This demonstrates that a pseudogapped state can coexist with a Hall carrier density of $\approx 1 + x$, conventionally interpreted as a large closed Fermi surface. We further show that for $x = 0.2$, the PG vanishes around $T^* = 200$ K, comparable to T^* of cuprates and to the Néel transition temperature of the undoped compounds.

Fig. 1 illustrates the doping dependence of the electronic structure of $\text{Sr}_{2-x}\text{La}_x\text{IrO}_4$ from the pristine compound to $x = 0.2$. Incoherent spectral weight near the Fermi energy E_F first appears at $x = 0.02$. However, a defined PG state with coherent Fermi arcs stretching

from the nodal $(0,0) - (\pi/2, \pi/2)$ direction and evolving into incoherent antinodal excitations only emerges at $x = 0.1$. The transition from an insulating to a pseudogapped state and the persistence of the nodal-antinodal dichotomy up to $x = 0.2$ are evident from the energy distribution curves (EDCs) in Fig. 1g,h. EDCs at the antinode show that although the leading edge of spectral weight shifts closer to E_F with increasing doping, a gap persists across the entire doping range. In contrast, nodal EDCs display the Fermi-Dirac cutoff of ungapped excitations for $x = 0.1$ and $x = 0.2$. Notably, the quasiparticle peak – nearly absent for $x = 0.1$ – becomes well-defined at $x = 0.2$. This is a signature of a striking increase of the nodal quasiparticle coherence with doping. These ARPES signatures of the PG state of Sr_2IrO_4 are highly reminiscent of hole doped cuprates. Yet there are two key differences. First, the FS in Sr_2IrO_4 is electron-like and centered at $(0,0)$, contrasting with the hole-like FS at (π, π) of the cuprates. Second, a doubling of the in-plane unit cell arising from a rotation of the oxygen octahedra causes a back folding of the FS in $\text{Sr}_{2-x}\text{La}_x\text{IrO}_4$ [15, 24, 25].

The emergence of a distinct coherent nodal quasiparticle peak from the broad incoherent features dominating

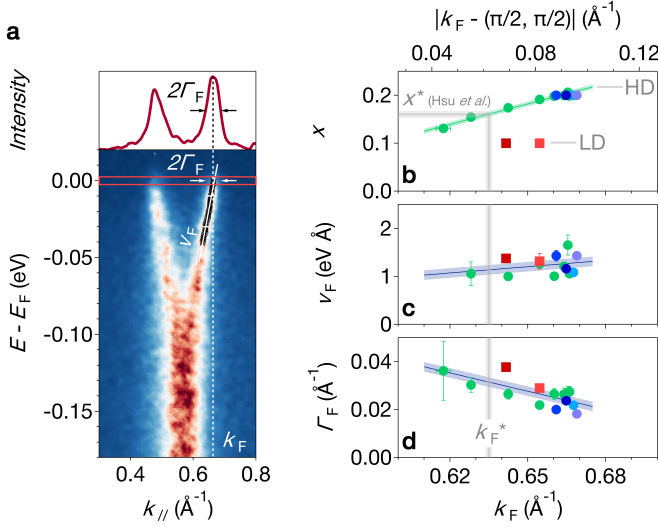


FIG. 2. **Continuous evolution of the electronic structure of $\text{Sr}_{2-x}\text{La}_x\text{IrO}_4$ with doping.** **a** Experimental definition of Fermi momentum k_F , Fermi velocity v_F , and scattering rate at the Fermi energy Γ_F . See methods for details. **b** Lanthanum concentration x versus Fermi momentum k_F . The green markers represent experimental data measured on a single HD sample which showed a smooth spatial variation of the La doping (see Supplementary Information A). A linear fit of these data (green line) defines the critical Fermi momentum k_F^* corresponding to the critical chemical doping x^* of Ref. [1] (light grey line). k_F measurements on other samples are represented by different colored markers - red squares for lightly doped (LD) and blue circles for highly doped (HD) samples. **c** Fermi velocity v_F and **d** scattering rate at the Fermi energy Γ_F as a function of the Fermi momentum k_F with standard deviations presented as bars. Shaded lines are linear fits of the experimental data.

the spectra at half-filling is also a key feature of pseudogapped cuprates. There, it appears at doping levels deep into the superconducting state but below the critical doping where the PG terminates [26, 27]. This indicates that our highly doped iridates are approaching the pseudogap doping boundary, and that further doping could lead to the predicted ungapped but still nodal-antinodal differentiated state [28]. It further highlights the conspicuous lack of superconductivity throughout the iridate pseudogap phase.

Fig. 2 quantifies the evolution of the electronic structure of $\text{Sr}_{2-x}\text{La}_x\text{IrO}_4$ with doping. To this end, we measured several samples grown with two different procedures (see Methods): lightly doped (nominal doping $x = 0.1$) and highly doped (nominal doping $x = 0.2$) samples, referred to as LD and HD, respectively. Crucially, our HD samples come from the same batch as those measured by Hsu *et al.* [1], allowing for a straightforward comparison of results. We determined the precise La content x in both sets with energy-dispersive x-ray spectroscopy (EDX). These measurements revealed a slow variation in x near the edges of some HD samples.

We exploit this smooth gradient to track the doping dependence of the nodal electronic structure by combining the EDX analysis with spatially resolved μ -spot ARPES measurements (see Supplementary Information A). We first determine the nodal Fermi wave vector $k_F(x)$ (shown as $x(k_F)$ in Fig. 2b) from fits to momentum distribution curves (MDCs). This reveals a clear dichotomy between LD and HD samples, implying that in one or both cases, the itinerant carrier density differs from the La concentration. We will discuss this point in more detail in Fig. 3. Importantly though, for the HD samples, also studied by Hsu *et al.* [1], we observe a clean linear evolution of k_F with x , without any discontinuity at $x^* \simeq 0.16$. This allows for a precise determination of the critical nodal k_F^* corresponding to the critical doping x^* identified in Ref. [1].

We next determine the nodal Fermi velocity v_F and the scattering rate at the Fermi energy Γ_F from MDC fits (see Methods for details of the analysis). When plotted against k_F , rather than x (Fig. 2c,d), v_F and Γ_F of LD and HD samples collapse onto a single curve. This shows that k_F is a more reliable indicator of the electronic state than the La concentration.

As k_F and thus the effective electron doping increases, we only observe a small gradual increase in v_F , with no abrupt changes detected at k_F^* . The reduction of the scattering rate with increasing k_F is more pronounced, in line with the significant rise in nodal quasiparticle coherence observed between the LD, $x = 0.1$ and the HD, $x = 0.2$ samples (Fig. 1g). Fig. 2c,d suggest a continuous evolution of v_F and Γ_F across the critical doping k_F^* . However, we presently have few data points only with $k_F < k_F^*$ for which the Fermi velocity and scattering rate remain well defined. We thus cannot fully exclude a more pronounced change at k_F^* .

Hsu *et al.* reported a strong enhancement of the electronic specific heat coefficient γ of $\text{Sr}_{2-x}\text{La}_x\text{IrO}_4$ over an extended doping range of $x \simeq 0.12 - 0.17$. They further point out that their data show no signs of a logarithmic divergence of the specific heat, typical for quantum critical systems [1]. In a conventional quasi-2D metal, $\gamma \propto m^* \propto 1/v_F$ where m^* is the quasiparticle effective mass. An enhancement of γ thus corresponds to an enhanced effective mass m^* and a correspondingly reduced Fermi velocity v_F . Our data are difficult to reconcile with such an interpretation of the measured electronic specific heat. Specifically, Fig. 2c shows that the nodal Fermi velocity remains nearly constant from x^*/k_F^* up to the highest doping of $x = 0.2$. In contrast Hsu *et al.* report a roughly 6-fold decrease of γ over the same doping range. Our direct measurements of the Fermi surface further exclude a Lifshitz transition and associated divergence in the single particle density of states in the relevant doping range.

In Fig. 3a,b we quantify the spectral weight suppression in the PG state along the FS (see Supplemen-

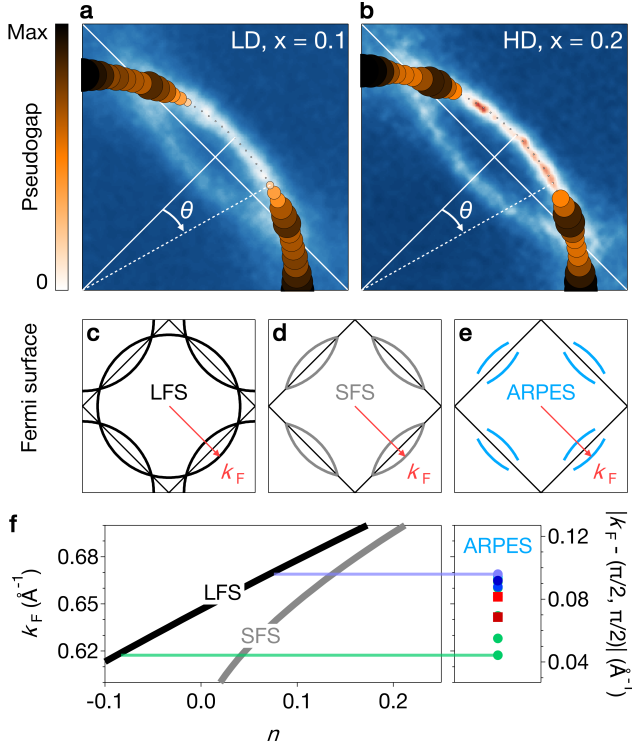


FIG. 3. **Pseudogap state of $\text{Sr}_{2-x}\text{La}_x\text{IrO}_4$.** **a,b** Spectral weight suppression in the PG (markers) overlaid on a quadrant of the Fermi surface for $x = 0.1$ and $x = 0.2$. **c** Schematic representation of the large (LFS) and **d** small (SFS) Fermi surface scenarios. **e** Sketch of the actual Fermi surface measured by ARPES. **f** Left: carrier density per Ir n versus Fermi momentum k_F in the large (black line) and small (grey line) scenarios. Right: range of k_F measured by ARPES in this study for samples with x between 0.1 and 0.2.

tary Information B for details). This shows an extended ungapped region stretching out from the nodal point up to $\theta \approx 13.5^\circ$ for $x = 0.1$ and $\theta \approx 18^\circ$ for $x = 0.2$, slightly larger than observed in overdoped $\text{Bi}_2\text{Sr}_2\text{CaCu}_2\text{O}_{8+\delta}$ [29]. Importantly though, the PG sets on deep into the nodal lens pockets for both $x = 0.1$ (LD sample) and $x = 0.2$ (HD sample). Hence, no conventional closed Fermi surface emerges up to the highest doping of $x = 0.2$. Instead, we find disconnected Fermi arcs extending out from the node, as illustrated schematically in Fig. 3e.

Hsu *et al.* interpret the Hall carrier density crossover from $n_H = 1 + x$ at high doping to $n_H = x$ at low doping as a reconstruction of a conventional large FS (LFS) upon entering the PG phase. An ungapped LFS – illustrated in Fig. 3c – has a well defined relation of Fermi wave vector k_F and carrier density per Ir n defined by the Luttinger theorem and shown as a black line in Fig. 3f. A simplified scenario for the PG phase is a small FS (SFS) consisting only of the lens-like nodal electron pockets while the antinodal hole pockets are gapped (Fig. 3d).

Our data question the applicability of these scenarios.

Assuming a closed SFS appears arbitrary, given that the PG extends deep into the lens-like contours of the Fermi surface maps (Fig. 3a,b). Moreover, within a LFS scenario – commonly used in cuprates – our experimental k_F values for La concentrations $0.1 < x < 0.2$ translate into carrier densities $-0.09 < n < 0.07$, nearly symmetric around zero doping.

A discrepancy of itinerant carrier densities and dopant concentration it not unusual. It can arise from co-doping from a slightly off-stoichiometric oxygen content or from a partial localization of doped electrons, as it is observed for instance in SrTiO_3 2D electron gases [30]. However, obtaining effective hole doping from substituting Sr by La is difficult to rationalize. Moreover, a LFS scenario places the evidently metallic state of the LD, $x = 0.1$ sample (Fig. 1c, Fig. 3a) at $n \simeq 0$ (half filling), which does not appear plausible. This suggests that the Luttinger theorem does not apply in the pseudogapped state of $\text{Sr}_{2-x}\text{La}_x\text{IrO}_4$.

It further highlights that care must be taken when comparing doping values of iridates and cuprates. Applying a LFS scenario, all $\text{Sr}_{2-x}\text{La}_x\text{IrO}_4$ samples studied in our work and by Hsu *et al.* [1] are heavily underdoped in the sense that n is significantly smaller than optimal doping in cuprates ($p \simeq 0.15$). At the same time, our $\text{Sr}_{2-x}\text{La}_x\text{IrO}_4$ samples with $x \simeq 0.2$ are overdoped in the sense that they have a large Hall carrier density $n_H \simeq 1 + x$ [1], which, in cuprates, is observed only above $p^* \simeq 0.19$ [7, 8].

In Fig. 4a we show the temperature evolution of the antinodal spectral function at the highest doping $x = 0.2$ ($k_F \simeq 0.67 \text{ \AA}^{-1}$). The clear gap, persisting all along the antinodal direction at $T = 6 \text{ K}$, gradually becomes less pronounced as temperature increases and completely disappears by $T = 235 \text{ K}$.

The EDCs at the antinodal k_F , shown in Fig. 4b over a large energy range, suggest that the PG disappears primarily by a gradual loss of coherent spectral weight. Similar behavior was reported in cuprates below the critical hole doping p^* [31]. Intriguingly though, here it is observed at a doping above x^* where the Hall carrier density is $\simeq 1 + x$ [1].

Measurements along the Brillouin zone diagonal (see Supplementary Information C) show that the nodal quasiparticle peak is more resilient and persists up to the highest temperature, albeit broadened. We finally note that low-temperature spectra taken immediately after the temperature-dependent measurements, as shown in Supplementary Information C, exhibit similar features to those observed before the temperature cycle. This rules out that the PG disappears in the data because of aging effects.

The vanishing PG further leads to a redistribution of spectral weight W_F along the Fermi surface (see Methods for the determination of W_F). Fig. 4d shows that the temperature dependence of W_F sets on abruptly at

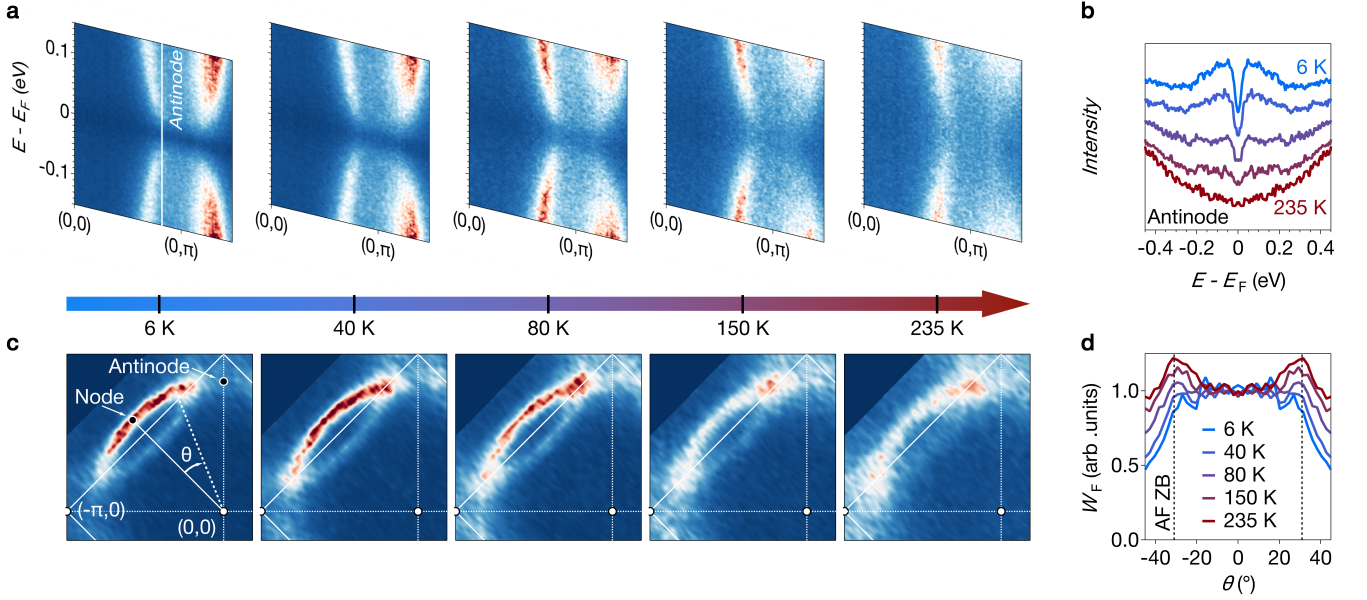


FIG. 4. **Temperature closure of the pseudogap for $x = 0.2$.** **a** Temperature dependence of the symmetrized band dispersion in the antinodal direction. **b** EDCs at the antinode (offset for clarity). **c** Temperature evolution of the Fermi surface. **d** Temperature dependence of the spectral weight W_F along the Fermi surface. The angle θ is defined in panel (c). Data were averaged over $\pm\theta$. See Methods for the procedure used to extract W_F . The dashed black lines shows the antiferromagnetic Brillouin zone boundary (AF ZB).

$\theta \simeq 18^\circ$ where the ungapped Fermi arc ends. Increasing the angle further, W_F first shows a local maximum around $\theta \simeq 31^\circ$ where the Fermi arc and its back-folded replica cross before it decreases towards the antinode. The suppression of weight towards the antinode is strongest at low temperature and gradually disappears as the highest temperature is approached. At the same time, the precise position of the local maximum shifts slightly in angle, consistent with a PG extending into the lens-like Fermi surface contour.

We remark that the PG reported in Ref. [23] for surface K-doped Sr_2IrO_4 appears to be more fragile than the PG of bulk La-doped $\text{Sr}_{2-x}\text{La}_x\text{IrO}_4$. In the K/ Sr_2IrO_4 system the PG was observed to fully close at a K coverage of ~ 0.85 ML where $k_F \simeq 0.67 \text{ \AA}^{-1}$. Our data show that at the same k_F , the PG clearly remains open in bulk doped samples. Moreover, the temperature boundary of $T^* \simeq 200$ K found here for $x = 0.2$ is significantly higher than the maximal $T^* = 70 \text{ K} - 110 \text{ K}$ at the K/ Sr_2IrO_4 interface observed at a lower doping (coverage of $0.7 \text{ ML} / k_F \simeq 0.655 \text{ \AA}^{-1}$). In addition, surface doped Sr_2IrO_4 shows an apparent d -wave gap, suggesting potential high-temperature surface superconductivity [32, 33]. Our data on bulk doped samples exclude a d -wave gap of similar magnitude and temperature dependence over the entire doping/ k_F range studied in Refs. [32, 33].

The temperature boundary of the PG in bulk electron-doped iridates observed here is strikingly similar to T^* in

cuprates [34, 35]. This is intriguing considering the much lower on-site repulsion U and stronger spin-orbit coupling λ_{SOC} in iridates [19, 36, 37] as well as the absence of superconductivity in the samples studied here [1, 18]. On the other hand, iridates and cuprates show similar energy scales in the magnetic sector. Magnons in undoped Sr_2IrO_4 disperse up to $\sim 205 \text{ meV}$ at $(\pi, 0)$ [19], comparable to the $\sim 320 \text{ meV}$ in La_2CuO_4 [38]. Moreover, spin fluctuations in both iridates [20, 39] and cuprates [40, 41] are known to persist up to high doping. These experimental findings point to an important role of short range antiferromagnetic spin fluctuations in the pseudogap physics of $\text{Sr}_{2-x}\text{La}_x\text{IrO}_4$. In turn, this provides further evidence for the importance of AF correlations for the PG in cuprates, which is also seen in numerical solutions of the Hubbard model [28, 42–46].

We further note a pronounced asymmetry between electron- and hole-doped iridates. A recent study of hole-doped $\text{Sr}_{1.93}\text{K}_{0.07}\text{IrO}_4$ films found a conventional large FS, in sharp contrast to the PG state of $\text{Sr}_{2-x}\text{La}_x\text{IrO}_4$ [47]. This is reminiscent of differences observed in hole- and electron-doped cuprates, although it remains unclear whether the underlying origins are similar. Indeed, both the orbitals involved and the nature of the insulating ground state are different: Cu e_g and O $2p$ orbitals with a large charge-transfer gap for the cuprates, spin-orbitally entangled Ir t_{2g} orbitals with small putative Mott-Hubbard gap in the iridate. Consequently, in cuprates doped holes have a different orbital character

than doped electrons [48], while they have different internal degrees of freedom in iridates and thus a different motion in their local magnetic environment [49].

In summary, our ARPES measurements of highly doped $\text{Sr}_{2-x}\text{La}_x\text{IrO}_4$ samples show a smooth evolution of the electronic structure up to the highest doping of $x \simeq 0.2$. Most importantly, we find that the anisotropic PG of $\text{Sr}_{2-x}\text{La}_x\text{IrO}_4$ persists up to $x = 0.2$ and thus beyond the crossover to a large Hall carrier density $\simeq 1 + x$ reported by Hsu *et al.* at a critical doping $x^* \simeq 0.16$. In cuprates, the cross over of the Hall density from $\simeq x$ to $\simeq 1 + x$ occurs at – or very close to – the critical doping p^* where the PG ends [7, 8]. Our work, taken together with the results of Hsu *et al.*, shows that iridates differ in this crucial aspect of PG phenomenology. At high doping, a large Hall carrier density $\simeq 1 + x$ coexists in iridates with an anisotropic pseudogap suppressing the antinodal spectral weight. Understanding the nature of this unusual state will require further experimental and theoretical work.

METHODS

Crystal growth

Single crystals with less than $x = 0.11$ lanthanum content (LD samples) were grown using a conventional flux cooling method, detailed elsewhere [15]. The lanthanum was measured by energy-dispersive X-ray spectroscopy and electron probe X-ray microanalysis. A flux evaporation method was used for crystals with high lanthanum concentrations (HD samples). For $x = 0.2$, SrCl_2 (Alfa Aesar, anhydrous, 2N₅) flux was combined with SrCO_3 (Sigma Aldrich, 4N), IrO_2 (Alfa Aesar, 3N) and La_2O_3 (Sigma Aldrich, 4N) in the ratio $\text{IrO}_2 + 8.5\text{SrCl}_2 + 1.44\text{SrCO}_3 + 0.36\text{La}_2\text{O}_3$. The SrCO_3 was dried at 600 °C and La_2O_3 at 1000 °C for 24 h. 0.83 g of IrO_2 was used for the successful attempts. All materials were ground in an agate mortar and pestle for twenty minutes and loaded into a 30 mL platinum crucible with a loose platinum lid. The crucible was loaded into a standard box furnace at 700 °C, ramped to 1350 °C in 3 h and held for 30 h. The furnace was then cooled to 800 °C at 4 °C/min, the crucible was removed, and air quenched to room temperature.

The crucible held a mixture of phases, including large (< 2 mm), square platelet samples (perhaps twenty per batch) and iridium metal. Little flux remained in the crucible, and the crystals were removed by soaking in warm water. There were often several morphologies, including triangular-platelet and square-platelet. Interestingly, the square-platelet crystals were consistently above $x = 0.16$ La content, while the triangular-platelet crystals were less than $x = 0.11$. The successful method was highly susceptible to synthesis conditions. Variations in starting mass, time baking, crucible volume and temperature

could all affect the outcome, preventing crystal growth of high La concentrations. The baking time needed to be long enough for the majority of the flux to evaporate, driving the growth of large crystals. The temperature window of successful growth was small, perhaps twenty degrees Celsius, vital to achieve high doping. Essentially, the intermediate oxidation state of the iridium required for high lanthanum doping is stabilised by temperature and chemical environment. If the temperature is too low, the iridium will not be sufficiently reduced, and if it is too high, the flux will evaporate too quickly, and the iridium will be reduced to metal. Successful reproduction of our method will require fine-tuning individual set-ups to optimise the temperature and starting mass/growth time.

ARPES measurements

Angle-Resolved Photoemission Spectroscopy (ARPES) experiments were performed at the I05 beamline (Diamond Light Source), the BLOCH beamline (Max IV), and the SIS beamline (Swiss Light Source). Samples were cleaved in ultra-high vacuum conditions ($P < 10^{-10}$ mbar) and at low temperatures ($T \simeq 50$ K for insulating samples, $T \leq 20$ K for conducting samples). Measurements were carried out using photon energies of $h\nu = 68$ eV or 100 eV, with an energy resolution ranging from 10 meV to 30 meV, depending on the specific measurement. The Fermi level was calibrated from reference measurements on a polycrystalline Au sample.

Details on data analysis

The data from undoped and lightly doped samples ($x \leq 0.1$) shown in Fig. 1 are extracted from the dataset of Ref. [15]. All the Fermi surface maps were obtained by integrating the measured intensity in the range $E_F \pm 5$ meV.

Fermi momenta k_F and scattering rates at the Fermi energy Γ_F , depicted in Fig. 2b-d, were obtained by fitting nodal Momentum Distribution Curves (MDCs) integrated over the range $E = E_F \pm 2.5$ meV. The MDCs, extending over the entire Brillouin zone, were modeled using four Lorentzian peaks with a second-order polynomial background, convolved with a Gaussian profile of full width at half maximum $\Delta E/v_F$ where ΔE is the energy resolution and v_F the Fermi velocity. The Fermi velocity v_F in Fig. 2c was obtained from linear fits of the MDC peak dispersion between $E_F - 30$ meV and $E_F - 10$ meV. Where available, the values of k_F , Γ_F , and v_F extracted from both sides of the Γ points were averaged.

To determine the pseudogap area as a function of the angle θ in Fig. 3a, we first removed a second-order polynomial background defined far from E_F (typically from $E - E_F = -0.3$ eV to $E - E_F = -0.05$ eV) to EDCs averaged over the range $k_F \pm 0.015 \text{ \AA}^{-1}$ for every Fermi surface angle θ . The background-subtracted symmetrized

EDCs relative to E_F were fitted with a Gaussian profile, the area of which were averaged for $\pm\theta$ and define the pseudogap spectral weight suppression.

The spectral weight at the Fermi level W_F shown in Fig. 4d was obtained by averaging the measured intensity in the range $E_F \pm 10$ meV and $k_F \pm 0.015 \text{ \AA}^{-1}$ at $\pm\theta$ for $\theta \in [-45^\circ, 45^\circ]$. For each temperature T , this quantity was normalised by the average nodal spectral weight $W_F(\theta \in [0^\circ, \pm 5^\circ], T)$.

DATA AVAILABILITY

The datasets used or analyzed during the current study are available from the corresponding authors upon reasonable request.

ACKNOWLEDGMENTS

We thank D. van der Marel and K. Wohlfeld for discussion. This work was supported by the Swiss National Science Foundation grants 146995, 165791, 184998. We acknowledge Diamond Light Source for time on Beamline I05 under Proposals SI10348, SI12404, SI17381. We acknowledge MAX IV Laboratory for time on Beamline Bloch under Proposal No. 20220192 and 20231600. Research conducted at MAX IV, a Swedish national user facility, is supported by the Swedish Research Council under Contract No. 2018-07152, the Swedish Governmental Agency for Innovation Systems under Contract No. 2018-04969, and Formas under Contract No. 2019-0249. We acknowledge the Paul Scherrer Institut, Villigen, Switzerland for provision of synchrotron radiation beamtime at the SIS beamline of the SLS.

AUTHOR CONTRIBUTIONS

F.B. and A.T. initiated and coordinated the project. A.d.l.T. and R.S.P. grew the crystals. Y.A., A.d.l.T., S.McK.W., M.S., G.G., A.H., S.M., E.C., S.R., F.Y.B., A.T. and F.B. performed the ARPES measurements with support from M.R., N.C.P., M.S., J.O., C.P., T.K.K., P.D. and M.H. Y.A. analyzed the data and prepared the figures with support from A.T. and F.B. Y.A., A.T. and F.B. wrote the paper with input from all authors.

COMPETING INTERESTS

The authors declare no competing interests.

* yann.alexanian@unige.ch

- [1] Y.-T. Hsu, A. Rydh, M. Berben, C. Duffy, A. de la Torre, R. S. Perry, and N. E. Hussey, Carrier density crossover and quasiparticle mass enhancement in a doped 5d mott insulator, *Nature Physics* **20**, 1596 (2024).
- [2] M. R. Norman, H. Ding, M. Randeria, J. C. Campuzano, T. Yokoya, T. Takeuchi, T. Takahashi, T. Mochiku, K. Kadowaki, P. Guptasarma, and D. G. Hinks, Destruction of the fermi surface in underdoped high- T_c superconductors, *Nature* **392**, 157 (1998).
- [3] K. M. Shen, F. Ronning, D. H. Lu, F. Baumberger, N. J. C. Ingle, W. S. Lee, W. Meevasana, Y. Kohsaka, M. Azuma, M. Takano, H. Takagi, and Z.-X. Shen, Nodal Quasiparticles and Antinodal Charge Ordering in $\text{Ca}_{2-x}\text{Na}_x\text{CuO}_2\text{Cl}_2$, *Science* **307**, 901 (2005).
- [4] P. A. Lee, N. Nagaosa, and X.-G. Wen, Doping a mott insulator: Physics of high-temperature superconductivity, *Reviews of Modern Physics* **78**, 17 (2006).
- [5] M. Civelli, M. Capone, S. S. Kancharla, O. Parcollet, and G. Kotliar, Dynamical breakup of the fermi surface in a doped mott insulator, *Physical Review Letters* **95** (2005).
- [6] G. Sordi, A. Amaricci, and M. J. Rozenberg, Metal-insulator transitions in the periodic anderson model, *Physical Review Letters* **99** (2007).
- [7] C. Proust and L. Taillefer, The remarkable underlying ground states of cuprate superconductors, *Annual Review of Condensed Matter Physics* **10**, 409 (2019).
- [8] S. Badoux, W. Tabis, F. Laliberté, G. Grissonnanche, B. Vignolle, D. Vignolles, J. Béard, D. A. Bonn, W. N. Hardy, R. Liang, N. Doiron-Leyraud, L. Taillefer, and C. Proust, Change of carrier density at the pseudogap critical point of a cuprate superconductor, *Nature* **531**, 210 (2016).
- [9] C. Putzke, S. Benhabib, W. Tabis, J. Ayres, Z. Wang, L. Malone, S. Licciardello, J. Lu, T. Kondo, T. Takeuchi, N. E. Hussey, J. R. Cooper, and A. Carrington, Reduced hall carrier density in the overdoped strange metal regime of cuprate superconductors, *Nature Physics* **17**, 826 (2021).
- [10] B. J. Kim, H. Jin, S. J. Moon, J.-Y. Kim, B.-G. Park, C. S. Leem, J. Yu, T. W. Noh, C. Kim, S.-J. Oh, J.-H. Park, V. Durairaj, G. Cao, and E. Rotenberg, Novel $J_{\text{eff}} = 1/2$ mott state induced by relativistic spin-orbit coupling in Sr_2IrO_4 , *Physical Review Letters* **101**, 076402 (2008).
- [11] B. J. Kim, H. Ohsumi, T. Komesu, S. Sakai, T. Morita, H. Takagi, and T. Arima, Phase-Sensitive Observation of a Spin-Orbital Mott State in Sr_2IrO_4 , *Science* **323**, 1329 (2009).
- [12] H. Jin, H. Jeong, T. Ozaki, and J. Yu, Anisotropic exchange interactions of spin-orbit-integrated states in Sr_2IrO_4 , *Physical Review B* **80**, 075112 (2009).
- [13] D. Choi, C. Yue, D. Azoury, Z. Porter, J. Chen, F. Petocchi, E. Baldini, B. Lv, M. Mogi, Y. Su, S. D. Wilson, M. Eckstein, P. Werner, and N. Gedik, Light-induced insulator-metal transition in Sr_2IrO_4 reveals the nature of the insulating ground state, *Proceedings of the National Academy of Sciences* **121**, e2323013121 (2024).
- [14] F. Wang and T. Senthil, Twisted hubbard model for Sr_2IrO_4 : Magnetism and possible high temperature su-

- perconductivity, *Physical Review Letters* **106**, 136402 (2011).
- [15] A. de la Torre, S. McKeown Walker, F. Bruno, S. Ricc, Z. Wang, I. Gutierrez Lezama, G. Scheerer, G. Girit, D. Jaccard, C. Berthod, T. Kim, M. Hoesch, E. Hunter, R. Perry, A. Tamai, and F. Baumberger, Collapse of the Mott Gap and Emergence of a Nodal Liquid in Lightly Doped Sr_2IrO_4 , *Physical Review Letters* **115**, 176402 (2015).
 - [16] V. Brouet, J. Mansart, L. Perfetti, C. Piovera, I. Vobornik, P. Le Fvre, F. Bertran, S. C. Riggs, M. C. Shapiro, P. Giraldo-Gallo, and I. R. Fisher, Transfer of spectral weight across the gap of Sr_2IrO_4 induced by the doping, *Physical Review B* **92**, 081117(R) (2015).
 - [17] S. Peng, C. Lane, Y. Hu, M. Guo, X. Chen, Z. Sun, M. Hashimoto, D. Lu, Z.-X. Shen, T. Wu, X. Chen, R. S. Markiewicz, Y. Wang, A. Bansil, S. D. Wilson, and J. He, Electronic nature of the pseudogap in electron-doped Sr_2IrO_4 , *npj Quantum Materials* **7**, 58 (2022).
 - [18] K. Wang, N. Bachar, J. Teyssier, W. Luo, C. W. Rischau, G. Scheerer, A. de la Torre, R. S. Perry, F. Baumberger, and D. van der Marel, Mott transition and collective charge pinning in electron doped Sr_2IrO_4 , *Physical Review B* **98**, 045107 (2018).
 - [19] J. Kim, D. Casa, M. H. Upton, T. Gog, Y.-J. Kim, J. F. Mitchell, M. van Veenendaal, M. Daghofer, J. van den Brink, G. Khaliullin, and B. J. Kim, Magnetic excitation spectra of Sr_2IrO_4 probed by resonant inelastic x-ray scattering: Establishing links to cuprate superconductors, *Physical Review Letters* **108**, 177003 (2012).
 - [20] D. Pincini, J. G. Vale, C. Donnerer, A. de la Torre, E. C. Hunter, R. Perry, M. Moretti Sala, F. Baumberger, and D. F. McMorro, Anisotropic exchange and spin-wave damping in pure and electron-doped Sr_2IrO_4 , *Physical Review B* **96**, 075162 (2017).
 - [21] J. Saylor, L. Takacs, C. Hohenemser, J. I. Budnick, and B. Chamberland, Nel temperature of stoichiometric La_2CuO_4 , *Physical Review B* **40**, 6854 (1989).
 - [22] S. M. Hayden, G. Aeppli, R. Osborn, A. D. Taylor, T. G. Perring, S.-W. Cheong, and Z. Fisk, High-energy spin waves in La_2CuO_4 , *Physical Review Letters* **67**, 3622 (1991).
 - [23] Y. K. Kim, O. Krupin, J. D. Denlinger, A. Bostwick, E. Rotenberg, Q. Zhao, J. F. Mitchell, J. W. Allen, and B. J. Kim, Fermi arcs in a doped pseudospin-1/2 Heisenberg antiferromagnet, *Science* **345**, 187 (2014).
 - [24] M. K. Crawford, M. A. Subramanian, R. L. Harlow, J. A. Fernandez-Baca, Z. R. Wang, and D. C. Johnston, Structural and magnetic studies of Sr_2IrO_4 , *Physical Review B* **49**, 9198 (1994).
 - [25] F. Ye, S. Chi, B. C. Chakoumakos, J. A. Fernandez-Baca, T. Qi, and G. Cao, Magnetic and crystal structures of Sr_2IrO_4 : A neutron diffraction study, *Physical Review B* **87**, 140406(R) (2013).
 - [26] K. M. Shen, F. Ronning, D. H. Lu, W. S. Lee, N. J. C. Ingle, W. Meevasana, F. Baumberger, A. Damascelli, N. P. Armitage, L. L. Miller, Y. Kohsaka, M. Azuma, M. Takano, H. Takagi, and Z.-X. Shen, Missing quasiparticles and the chemical potential puzzle in the doping evolution of the cuprate superconductors, *Physical Review Letters* **93**, 267002 (2004).
 - [27] D. Fournier, G. Levy, Y. Pennec, J. L. McChesney, A. Bostwick, E. Rotenberg, R. Liang, W. N. Hardy, D. A. Bonn, I. S. Elfimov, and A. Damascelli, Loss of nodal quasiparticle integrity in underdoped $\text{YBa}_2\text{Cu}_3\text{O}_{6+x}$, *Nature Physics* **6**, 905 (2010).
 - [28] A. Moutenet, A. Georges, and M. Ferrero, Pseudogap and electronic structure of electron-doped Sr_2IrO_4 , *Physical Review B* **97**, 155109 (2018).
 - [29] W. S. Lee, I. M. Vishik, K. Tanaka, D. H. Lu, T. Sasagawa, N. Nagaosa, T. P. Devereaux, Z. Hussain, and Z. X. Shen, Abrupt onset of a second energy gap at the superconducting transition of underdoped $\text{Bi}_2\text{Te}_2\text{Te}_2$, *Nature* **450**, 81 (2007).
 - [30] S. McKeown Walker, F. Y. Bruno, Z. Wang, A. de la Torre, S. Ricc, A. Tamai, T. K. Kim, M. Hoesch, M. Shi, M. S. Bahramy, P. D. C. King, and F. Baumberger, Carrier-Density Control of the SrTiO_3 (001) Surface 2D Electron Gas studied by ARPES, *Advanced Materials* **27**, 3894 (2015).
 - [31] S.-D. Chen, M. Hashimoto, Y. He, D. Song, K.-J. Xu, J.-F. He, T. P. Devereaux, H. Eisaki, D.-H. Lu, J. Zaanen, and Z.-X. Shen, Incoherent strange metal sharply bounded by a critical doping in $\text{Bi}_2\text{Te}_2\text{Te}_2$, *Science* **366**, 1099 (2019).
 - [32] Y. K. Kim, N. H. Sung, J. D. Denlinger, and B. J. Kim, Observation of a d-wave gap in electron-doped Sr_2IrO_4 , *Nature Physics* **12**, 37 (2015).
 - [33] Y. Yan, M. Ren, H. Xu, B. Xie, R. Tao, H. Choi, N. Lee, Y. Choi, T. Zhang, and D. Feng, Electron-doped Sr_2IrO_4 : An analogue of hole-doped cuprate superconductors demonstrated by scanning tunneling microscopy, *Physical Review X* **5**, 041018 (2015).
 - [34] T. Yoshida, M. Hashimoto, S. Ideta, A. Fujimori, K. Tanaka, N. Mannella, Z. Hussain, Z.-X. Shen, M. Kubota, K. Ono, S. Komiya, Y. Ando, H. Eisaki, and S. Uchida, Universal versus material-dependent two-gap behaviors of the high- T_c cuprate superconductors: Angle-resolved photoemission study of $\text{La}_{2-x}\text{Sr}_x\text{CuO}_4$, *Physical Review Letters* **103**, 037004 (2009).
 - [35] O. Cyr-Choinire, R. Daou, F. Lalibert, C. Collignon, S. Badoux, D. LeBoeuf, J. Chang, B. J. Ramshaw, D. A. Bonn, W. N. Hardy, R. Liang, J.-Q. Yan, J.-G. Cheng, J.-S. Zhou, J. B. Goodenough, S. Pyon, T. Takayama, H. Takagi, N. Doiron-Leyraud, and L. Taillefer, Pseudogap temperature T^* of cuprate superconductors from the nernst effect, *Physical Review B* **97**, 064502 (2018).
 - [36] S. J. Moon, H. Jin, W. S. Choi, J. S. Lee, S. S. A. Seo, J. Yu, G. Cao, T. W. Noh, and Y. S. Lee, Temperature dependence of the electronic structure of the $J_{\text{eff}} = 1/2$ mott insulator Sr_2IrO_4 studied by optical spectroscopy, *Physical Review B* **80**, 195110 (2009).
 - [37] Q. Wang, Y. Cao, J. A. Waugh, S. R. Park, T. F. Qi, O. B. Korneta, G. Cao, and D. S. Dessau, Dimensionality-controlled mott transition and correlation effects in single-layer and bilayer perovskite iridates, *Physical Review B* **87**, 245109 (2013).
 - [38] R. Coldea, S. M. Hayden, G. Aeppli, T. G. Perring, C. D. Frost, T. E. Mason, S.-W. Cheong, and Z. Fisk, Spin waves and electronic interactions in La_2CuO_4 , *Phys. Rev. Lett.* **86**, 5377 (2001).
 - [39] H. Gretarsson, N. Sung, J. Porras, J. Bertinshaw, C. Dietl, J. A. Bruin, A. Bangura, Y. Kim, R. Dinnebier, J. Kim, A. Al-Zein, M. Moretti Sala, M. Krisch, M. Le Tacon, B. Keimer, and B. Kim, Persistent paramagnons deep in the metallic phase of $\text{Sr}_{2-x}\text{La}_x\text{IrO}_4$, *Physical Review Letters* **117**, 107001 (2016).

- [40] B. Keimer, N. Belk, R. J. Birgeneau, A. Cassanho, C. Y. Chen, M. Greven, M. A. Kastner, A. Aharony, Y. Endoh, R. W. Erwin, and G. Shirane, Magnetic excitations in pure, lightly doped, and weakly metallic La_2CuO_4 , [Physical Review B](#) **46**, 14034 (1992).
- [41] G. Drachuck, E. Razzoli, G. Bazalitski, A. Kanigel, C. Niedermayer, M. Shi, and A. Keren, Comprehensive study of the spin-charge interplay in antiferromagnetic $\text{La}_{2-x}\text{Sr}_x\text{CuO}_4$, [Nature Communications](#) **5**, 3390 (2014).
- [42] B. Kyung, S. S. Kancharla, D. Sénéchal, A.-M. S. Tremblay, M. Civelli, and G. Kotliar, Pseudogap induced by short-range spin correlations in a doped mott insulator, [Physical Review B](#) **73**, 165114 (2006).
- [43] O. Gunnarsson, T. Schäfer, J. LeBlanc, E. Gull, J. Merino, G. Sangiovanni, G. Rohringer, and A. Toschi, Fluctuation diagnostics of the electron self-energy: Origin of the pseudogap physics, [Physical Review Letters](#) **114**, 236402 (2015).
- [44] W. Wu, M. Ferrero, A. Georges, and E. Kozik, Controlling feynman diagrammatic expansions: Physical nature of the pseudogap in the two-dimensional hubbard model, [Physical Review B](#) **96**, 041105(R) (2017).
- [45] H. Wang, S.-L. Yu, and J.-X. Li, Fermi arcs, pseudogap, and collective excitations in doped Sr_2IrO_4 : A generalized fluctuation exchange study, [Physical Review B](#) **91**, 165138 (2015).
- [46] F. Šimkovic, R. Rossi, A. Georges, and M. Ferrero, Origin and fate of the pseudogap in the doped Hubbard model, [Science](#) **385**, eade9194 (2024).
- [47] J. N. Nelson, C. T. Parzyck, B. D. Faeth, J. K. Kawasaki, D. G. Schlom, and K. M. Shen, Mott gap collapse in lightly hole-doped $\text{Sr}_{2-x}\text{K}_x\text{IrO}_4$, [Nature Communications](#) **11**, 2597 (2020).
- [48] N. P. Armitage, P. Fournier, and R. L. Greene, Progress and perspectives on electron-doped cuprates, [Rev. Mod. Phys.](#) **82**, 2421 (2010).
- [49] E. M. Pärschke, K. Wohlfeld, K. Foyevtsova, and J. van den Brink, Correlation induced electron-hole asymmetry in quasi- two-dimensional iridates, [Nature Communications](#) **8**, 686 (2017).

Supplementary Information for "Fermi surface and pseudogap in highly doped Sr_2IrO_4 "

Y. Alexanian,^{1,*} A. de la Torre,^{2,3} S. McKeown Walker,^{1,4} M. Straub,¹ G. Gatti,¹ A. Hunter,¹ S. Mandloi,¹ E. Cappelli,¹ S. Riccò,¹ F. Y. Bruno,⁵ M. Radovic,⁶ N. C. Plumb,⁶ M. Shi,⁶ J. Osiecki,⁷ C. Polley,⁷ T. K. Kim,⁸ P. Dudin,^{8,9} M. Hoesch,¹⁰ R. S. Perry,^{11,12} A. Tamai,¹ and F. Baumberger^{1,6}

¹*Department of Quantum Matter Physics, University of Geneva,
24 Quai Ernest-Ansermet, CH-1211, Geneva, Switzerland*

²*Department of Physics, Northeastern University, Boston, MA, 02115, USA*

³*Quantum Materials and Sensing Institute, Northeastern University, Burlington, MA, 01803 USA*

⁴*Laboratory of Advanced Technology, University of Geneva,
24 Quai Ernest-Ansermet, CH-1211, Geneva, Switzerland*

⁵*GFMC, Departamento de Física de Materiales, Universidad Complutense de Madrid, 28040 Madrid, Spain*

⁶*Swiss Light Source, Paul Scherrer Institut, CH-5232 Villigen PSI, Switzerland*

⁷*MAX IV Laboratory, Lund University, SE-211 00 Lund, Sweden*

⁸*Diamond Light Source, Harwell Campus, Didcot, OX11 0DE, United Kingdom*

⁹*Synchrotron SOLEIL, L'Orme des Merisiers, Saint Aubin-BP 48, 91192 Gif sur Yvette Cedex, France*

¹⁰*Deutsches Elektronen-Synchrotron DESY, Notkestraße 85, 22607 Hamburg, Germany*

¹¹*ISIS Pulsed Neutron and Muon Source, STFC Rutherford Appleton Laboratory,
Harwell Campus, Didcot, Oxon OX11 0QX, United Kingdom*

¹²*London Centre for Nanotechnology and Department of Physics and Astronomy,
University College London, London WC1E 6BT, United Kingdom*

(Dated: May 20, 2025)

A. SAMPLE CHARACTERIZATION AND DOPING DEPENDENCE

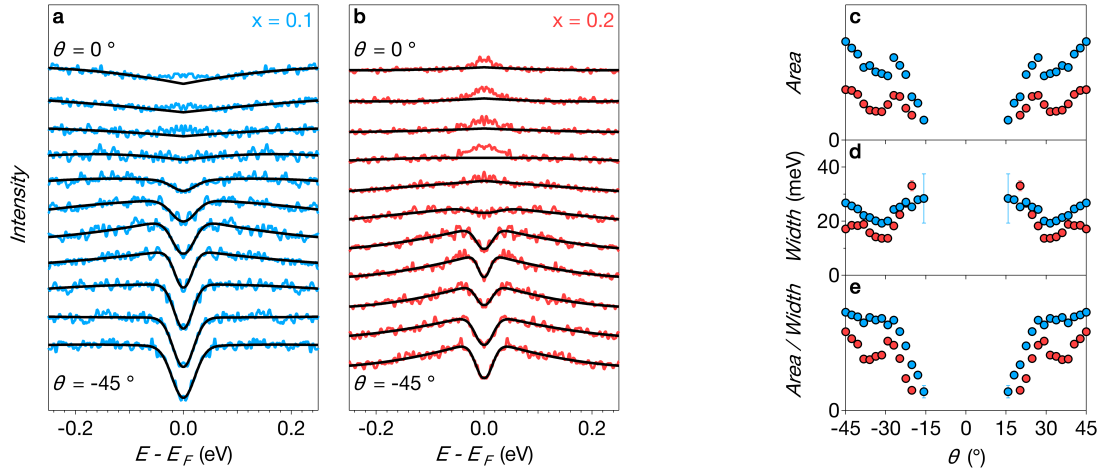
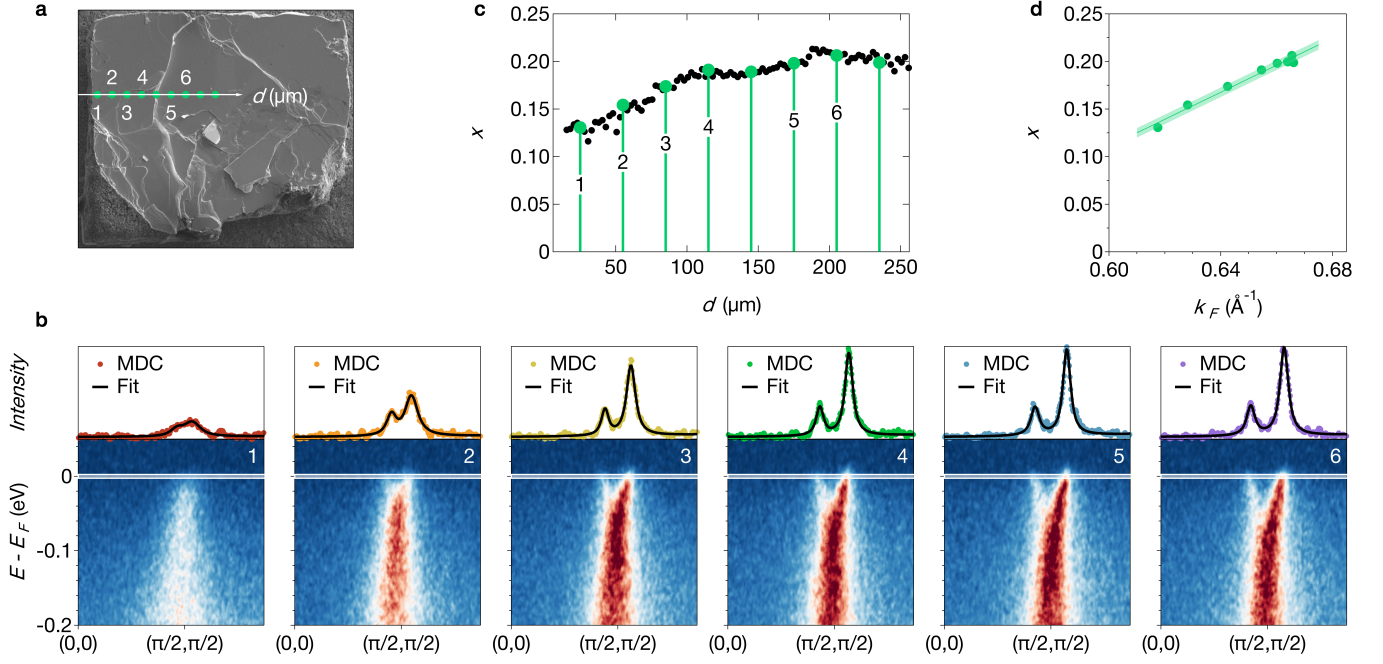
In Fig. S1, we present the evolution of the ARPES spectra of $\text{Sr}_{2-x}\text{La}_x\text{IrO}_4$ as a function of the ARPES spot position in one of our HD samples, which exhibits inhomogeneous chemical doping x . Spectra in the nodal direction measured at several points spaced by 30 μm (see Fig. S1a) are shown in Fig. S1b. Significant changes in the electronic structure near the Fermi energy are observed: the two branches around $(\pi/2, \pi/2)$, forming the lenses of the Fermi surface, are indistinguishable near the sample edge but become clearly visible towards its center. This evolution correlates with variations in the lanthanum concentration x along the line, as measured by energy-dispersive X-ray spectroscopy (EDX), and shown in Fig. S1c. Interestingly, we found that the Fermi momentum k_F (extracted from MDCs at $E = E_F$) increases linearly with the chemical doping value x (Fig. S1d). Although the chemical doping x cannot be directly related to electron doping (see main text), its evolution in a single type of sample reflects changes in electron doping. Finally, note that this spatial variation of x is typical for our HD samples, whereas LD samples exhibit a more homogeneous doping distribution.

B. ANGULAR DEPENDENCE OF THE PSEUDOGAP

In Fig. S2 we provide additional details on the determination of the angular dependence of the pseudogap shown in Fig. 3a of the main text. First, we fitted a second-order polynomial background $B(E - E_F)$ in the energy interval $-0.3 \text{ eV} \leq E - E_F \leq -0.05 \text{ eV}$ of the EDCs measured at k_F for various angles θ (each EDC corresponds to a color dot in Fig. 3a). We then removed the background of the EDCs and fitted the symmetrized remaining signal in the energy range $-0.05 \text{ eV} \leq E - E_F \leq 0.05 \text{ eV}$ with a Gaussian function defined as:

$$G(E - E_F) = \frac{A}{2\gamma\sqrt{\pi/\ln(16)}} \exp\left(-\left(\frac{E - E_F}{2\gamma}\right)^2 \ln(16)\right). \quad (\text{S1})$$

Examples of the EDCs and their total fits $B(E - E_F) + G(E - E_F)$ are shown in Fig. S2a for $x = 0.1$ and Fig. S2b for $x = 0.2$. The spectral weight suppression in the PG, shown in Fig. 3a of the main text, is defined as the area A . Figs. S2c,d,e show the area A together with the gap width γ , and the gap amplitude A/γ . Interestingly, our fits also indicate that it is the gap amplitude, rather than the gap width, that decreases as the node is approached. Lastly, note the presence of a local maximum (and corresponding local minimum) in the gap area (gap width) around $\pm 30^\circ$, where the primitive and backfolded bands cross.



C. COMPLEMENT ON THE TEMPERATURE DEPENDENCE

In Fig. S3 we present temperature-dependent measurements of the electronic structure of $\text{Sr}_{1.8}\text{La}_{0.2}\text{IrO}_4$ along the nodal direction. Symmetrized cuts from $T = 6\text{ K}$ to $T = 235\text{ K}$ (see Fig. S3a) reveal the absence of any gap within this temperature range, in stark contrast to the temperature-dependent pseudogap observed in the antinodal direction (see Fig. 4a of main text). Moreover, the nodal EDCs at different temperature, shown in Fig. S3b, demonstrate that the sharp quasiparticle peak visible at $T = 6\text{ K}$ broadens with increasing temperature but remains present up to the highest temperature measured. Notably, we observe no significant change when the pseudogap vanishes (between $T = 150\text{ K}$ and $T = 235\text{ K}$).

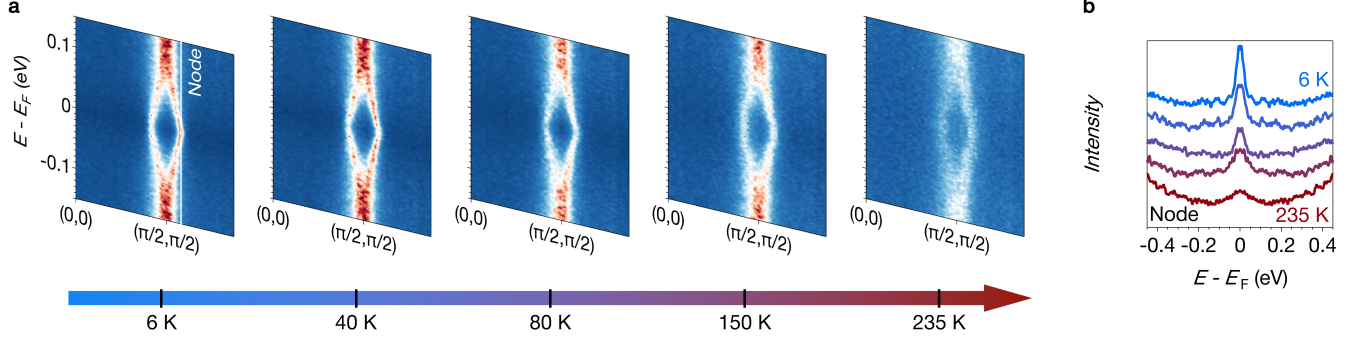


FIG. S3. **Temperature dependence of nodal ARPES spectra in $\text{Sr}_{1.8}\text{La}_{0.2}\text{IrO}_4$.** **a** Temperature dependence of the symmetrized band dispersion in the nodal direction. The node position is indicated by the white line. **b** EDCs at the node, shifted by a different constant intensity for each temperature.

Low-temperature measurements ($T = 20\text{ K}$) taken after the complete temperature cycle from $T = 6\text{ K}$ to $T = 235\text{ K}$ are shown in Fig. S4. Symmetrized cuts along both the nodal and antinodal directions (Figs. S4a,b) as well as the Fermi surface (Fig. S4c) are similar to those obtained at low temperature before the cycle (see Figs. 4 and S3). Most importantly, a pseudogap remains evident at the antinode, while no gap is observed at the node, ruling out any aging effect as an explanation for the pseudogap closure in our data.

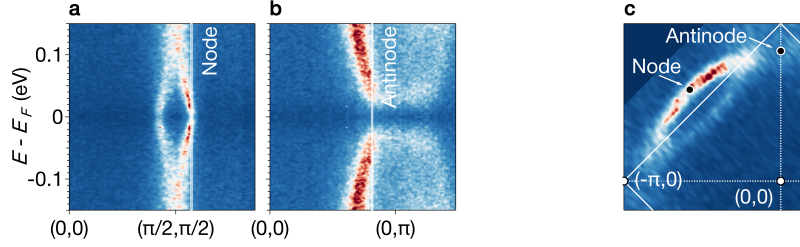


FIG. S4. **Low-temperature measurements of $\text{Sr}_{1.8}\text{La}_{0.2}\text{IrO}_4$ after a complete temperature cycle.** **a,b** Symmetrized cuts along the nodal and antinodal directions, respectively. **c** Fermi surface.